Received: 31 December 2021 | Revised: 6 March 2022 | Accepted: 15 March 2022

DOI: 10.1002/joc.7614

RESEARCH ARTICLE

International Journal of Climatology RMetS

# Moisture transport and water vapour budget over the Sahara Desert

**Li Zhuo** | **Liming Zhou**

Department of Atmospheric and Environmental Sciences, University at Albany, State University of New York, Albany, New York, USA

**Correspondence**
Liming Zhou, Department of Atmospheric and Environmental Sciences, University at Albany, State University of New York, 1400 Washington Avenue, Albany, NY 12222, USA.
Email: lzhou@albany.edu

**Funding information**
National Science Foundation, Grant/Award Number: AGS-1952745

**Abstract**

Previous studies documented that near-surface temperatures over the Sahara and Arabian deserts have been amplified in a warming climate, which is termed desert amplification (DA). DA has been linked possibly to the large-scale greenhouse effects associated with increasing water vapour. With very limited moisture availability over the driest desert, two key questions unanswered are the desert moisture sources and the relative contributions of thermodynamic and dynamic processes to the changes in moisture transport. In this study, the atmospheric water vapour budget over the Sahara Desert from 1981–2020 is analysed to address these two questions. Results indicate that the water vapour content over the Sahara Desert has increased significantly since 1981, primarily during the boreal summer and in the lower to middle troposphere. The water vapour budget analysis indicates that in the boreal summer, most of the added moisture is transported into the Sahara Desert through the intensifying northerly inflow across the northern boundary of the desert, while the other boundaries are all export channels. The northerly inward moisture transport is associated with the ridge in the lower troposphere and the Saharan high above the lower troposphere. Further analysis indicates that both dynamic and thermodynamic factors contribute to the increase of the inward moisture flux at the northern boundary, while the associated interannual variability is dominated by the dynamic component related to the circulation pattern changes. The changes of the circulation pattern in the lower troposphere are *manifested* as the westward extension of the low over the Arabian Peninsula and as the strengthening of the Saharan high above the lower troposphere, both contributing to the increase of the northerly inward moisture transport.

**KEYWORDS**

moisture transport, Sahara Desert, water vapour budget

## 1 | INTRODUCTION

The Sahara and Arabian deserts, the largest and driest deserts on Earth, have been argued to have experienced the largest warming rate in the low and middle latitudes (termed desert amplification or DA) based on global-scale analyses of observational, reanalysis and climate model datasets (Zhou *et al*., 2015; Zhou, 2016; Wei *et al*., 2017). Similar views were also documented by regional-scale studies (Cook and Vizy, 2015; Evan *et al*., 2015; Vizy and Cook, 2017; Cook *et al*., 2021). For example, based on observational and reanalysis datasets, Cook and Vizy (2015) reported that the warming rate of the surface temperature on the Sahara Desert is much larger than that in the tropical

  

regions. The Sahara Desert is also found to have expanded significantly in the past century (Thomas and Nigam, 2018), which is consistent with the concept of DA. The magnitude of DA is found to be strongest near the surface and decreases gradually with height (Wei *et al*., 2017; Zhou, 2021).

Research on the potential mechanisms driving the DA is still in the early stages (Thomas and Nigam, 2018; Zhou, 2021). Recent studies have attributed the DA likely to the enhanced downward longwave radiation induced by the increasing amounts of greenhouse gases (Evan *et al*., 2015; Cook and Vizy, 2015; Vizy and Cook, 2017; Zhou, 2016; 2021; Zhou *et al*., 2016; Zhou *et al*., 2021a; 2021b). Among the greenhouse gases, water vapour is found to play a big role in enhancing the downward longwave radiation over the deserts in response to a warmer and moister atmosphere. For instance, based on the observational and reanalysis datasets, Zhou *et al*. (2016) documented a negative logarithmic relationship between the total content of water vapour in the atmospheric column and the ratio of downward longwave radiation trend to the total water vapour content trend, indicating the largest efficiency in the greenhouse effect over the driest regions like the Sahara Desert. Using a heat and water vapour budget analysis, Evan *et al*. (2015) also attributed the increase of the temperature over the Sahara Desert to the enhanced greenhouse warming by moisture. By separating the DA into dry and wet seasons, Vizy and Cook (2017) found that during the wet season, it is the increased amounts of moisture over the Sahara Desert that drives the fast warming of the near-surface temperature.

The aforementioned studies, however, do not completely address one key question regarding the remote moisture transport and its variability over the Sahara Desert where the local moisture availability is very limited. Vizy and Cook (2017) qualitatively analysed the changes in circulation patterns over the Sahara Desert and found increased moisture transport into the Sahara Desert via the strengthening of the Sahara low/Saharan high system (Figure 11). However, a detailed quantitative analysis is still needed to examine the water vapour transport over the Sahara Desert, because there may be multiple mechanisms through which the moisture can be transported into the atmosphere over the desert. For example, it is long established that the African monsoon plays a significant role in the rainfall in the Sahel (Druyan, 2011; Monerie *et al*., 2016; Odoulami and Akinsanola, 2018; Akinsanola and Zhou, 2019a; 2019b) and the southern Sahara (Thomas and Nigam, 2018; Pausata *et al*., 2020). So the possibility that variations in the African monsoon may also have modified the moisture transported to the Sahara Desert cannot be ruled out. In addition, the change of the moisture content over a specific region could be driven by the dynamic or thermodynamic factors (Seager *et al*., 2010; Wang *et al*., 2017; Akinsanola and Zhou, 2019a; 2019b). Separating the dynamic and thermodynamic contributions to the increase of the Sahara Desert moisture also needs in-depth quantitative analysis.

Aiming at addressing the questions mentioned above and shedding some light on our understanding of the DA, here we conduct the water vapour budget analysis to analyse the moisture variability over the Sahara Desert. To our best knowledge, no such work has been done before. The paper is organized as follows. In section 2 we will discuss the data and methods used. The main results and discussion will be given in section 3. Section 3.1 provides an overview of the moisture trends over the Sahara Desert. Section 3.2 analyzes the results of the water vapour budget. Section 3.3 quantifies the relative contributions of the dynamic and thermodynamic processes to the inward moisture flux. Concluding remarks follow in section 4.

## 2 | DATA AND METHODS

In this paper, we define the Sahara Desert as the region located between 20°–30°N and 10°W–30°E, following previous studies (Harada *et al*., 2003; Cook and Vizy, 2015). We use two reanalysis datasets, including the fifth major global reanalysis produced by European Centre for Medium-Range Weather Forecasts (ERA5; Hersbach *et al*., 2020) and the Modern-Era Retrospective Analysis for Research and Applications, version 2 (MERRA-2; Gelaro *et al*., 2017), for the period 1981–2020. To calculate the moisture budget components, here we use 6-hourly fields of specific humidity ($q$), zonal and meridional winds ($u$, $v$) from ERA5 and MERRA-2 at a horizontal resolution of $1°\times1°$ and $0.5°\times0.625°$, respectively. We have also utilized the ERA5 data at the resolution of $0.25°\times0.25°$ and find that the results are similar. Monthly means quantities, such as horizontal winds, specific humidity and other calculated variables like moisture flux ($\rho q\vec{V}$), and geopotential heights, are aggregated to create the corresponding seasonal and annual mean variables. Here we classify June–August (JJA) as the boreal summer and December–February (DJF) as the boreal winter. The linear trend is calculated via least squares fitting and a two-tailed Student's $t$ test is used to test the significance of the trend.

Following previous studies (Sun and Wang, 2014; Wang *et al*., 2015; Dai *et al*., 2020; Mayer *et al*., 2021), the water vapour budget equation can be written as

$$\frac{1}{g}\frac{\partial}{\partial t}\int_{p_t}^{p_s} q\,dp = -\frac{1}{g}\int_{p_t}^{p_s}\nabla\cdot\left(q\vec{V}\right)dp + E - P + R, \qquad (1)$$

where $g$ is the gravitational constant, $q$ and $\vec{V}$ are the specific humidity and the horizontal wind vector, respectively, $p_s$ and $p_t$ are the pressure at the surface and top of the atmosphere, respectively. Here we set $p_t = 300\,\text{hPa}$.

The left term of Equation (1) is the time change of the total precipitable water (TPW) in a single atmospheric column. The first term on the right hand of Equation (1) is the vertically integrated moisture flux convergence (VIMFC). $E$ and $P$ are the surface evaporation and precipitation rates, respectively. $R$ is the residual term.

Using the 2D divergence theorem (Zangvil *et al.*, 2004; Jin *et al.*, 2011; Lamb *et al.*, 2012; Minallah and Steiner, 2021), VIMFC can be written as

$$\mathrm{VIMFC} = -\frac{1}{g}\int_{p_t}^{p_s} \nabla \cdot \left(q\vec{V}\right) dp = -\frac{1}{Ag}\int\int qV_n dl dp, \quad (2)$$

where $dl$ is the length of the grid along the latitude and longitude, $V_n$ is the wind vector projected to the normal direction of each boundary, and $A$ is the area of the integration region. The right-hand term of Equation (2) can be expressed in the form of the total net moisture fluxes across the four boundaries of the Sahara Desert,

$$-\frac{1}{Ag}\int\int qV_n dl dp = \frac{1}{A}(-\text{north flux} + \text{south flux} - \text{east flux} + \text{west flux}), \quad (3)$$

where the right-hand terms of Equation (3) represent the moisture flux across the northern, southern, eastern and western boundaries, respectively. For convenience, here we rewrite Equation (3) as

$$-\frac{1}{Ag}\int\int qV_n dl dp = F_{\text{north}} + F_{\text{south}} + F_{\text{east}} + F_{\text{west}}, \quad (4)$$

where $F_{\text{north}}$, $F_{\text{south}}$, $F_{\text{east}}$ and $F_{\text{west}}$ represent the moisture transport across the northern, southern, eastern and western boundaries, respectively.

To further quantify the relative contributions of thermodynamic and dynamic processes to the change of the moisture transports, here we decompose the moisture flux across a certain boundary into anomalies due to changes of wind and specific humidity respectively, following previous studies (Seager *et al.*, 2010; Wang *et al.*, 2017; Akinsanola and Zhou, 2019a):

$$\frac{1}{g}\int\int -qV_n dl dp = \frac{1}{g}\int\int -\overline{q}\,\overline{V}_n dl dp + \frac{1}{g}\int\int -q'^{\overline{V}_n} dl dp + \frac{1}{g}\int\int -\overline{q}V'_n dl dp + \frac{1}{g}\int\int -q'^{V'_n} dl dp, \quad (5)$$

where $\overline{V_n}$ and $\overline{q}$ are the 40-year (1981–2020) climatology of the wind normal to a specific boundary and specific humidity in a specific season or year, and $V'_n$ and $q'$ are the respective deviations from the 40-year climatology of each year or season. The term on the left-hand of Equation (5) is the moisture flux across a certain boundary. The first term on the right hand of Equation (5) is the average term, which is constant within 40 years. The second term and third term are the moisture flux anomalies caused by the thermodynamical (thermodynamic term) and dynamical processes (dynamic term), respectively. The last term can be neglected for both $q'$ and $V'_n$ are small deviations from the climatology (Wang *et al.*, 2017).

## 3 | RESULTS AND DISCUSSION

### 3.1 | Moisture trends in ERA5 and MERRA-2

Figure 1 displays the spatial distribution of JJA, DJF and annual TPW climatology in ERA5 (left) and MERRA-2 (right). The comparison between the left and right columns highlights the great similarity in TPW between the two reanalysis datasets over the Sahara Desert, especially for JJA and annual TPW. The differences in DJF TPW are relatively larger than the differences in JJA and annual TPW. However, as shown later, the moistening over the Sahara Desert mainly takes place in JJA and such differences in DJF will not matter much in our study.

The spatial patterns of JJA, DJF and annual TPW trends in ERA5 and MERRA-2 are shown in Figure 2. Comparing the left columns to the right columns, one can see that the two datasets display similar moistening trends in both the spatial patterns and magnitude. In JJA, both indicate positive TPW trends that are statistically significant at the 99% confidence level over most areas in the Sahel and the Sahara Desert (depicted as the rectangle box in blue), with the maximum of the magnitude located in the Sahel (Figure 2a,b). There is evidence of a significant moistening trend around the west coastline of the African land at 16°N in MERRA-2 (Figure 2b), which is absent in ERA5 (Figure 2a). However, this difference is out of the area of our study domain and thus will not influence our further analysis over the Sahara Desert. In DJF, neither ERA5 or MERRA-2 exhibits statistically significant moistening trends over the Sahara Desert (Figure 2c,d). The annual trends of TPW in ERA5 also correspond well to the trends in MERRA-2 in terms of the spatial patterns and magnitude, as both exhibit positive TPW trends over the Sahara Desert and the Sahel (Figure 2e,f). It is noteworthy that the spatial patterns of the annual TPW trends share great similarity with the JJA TPW trends in both ERA5 and MERRA-2 (Figure 2a,

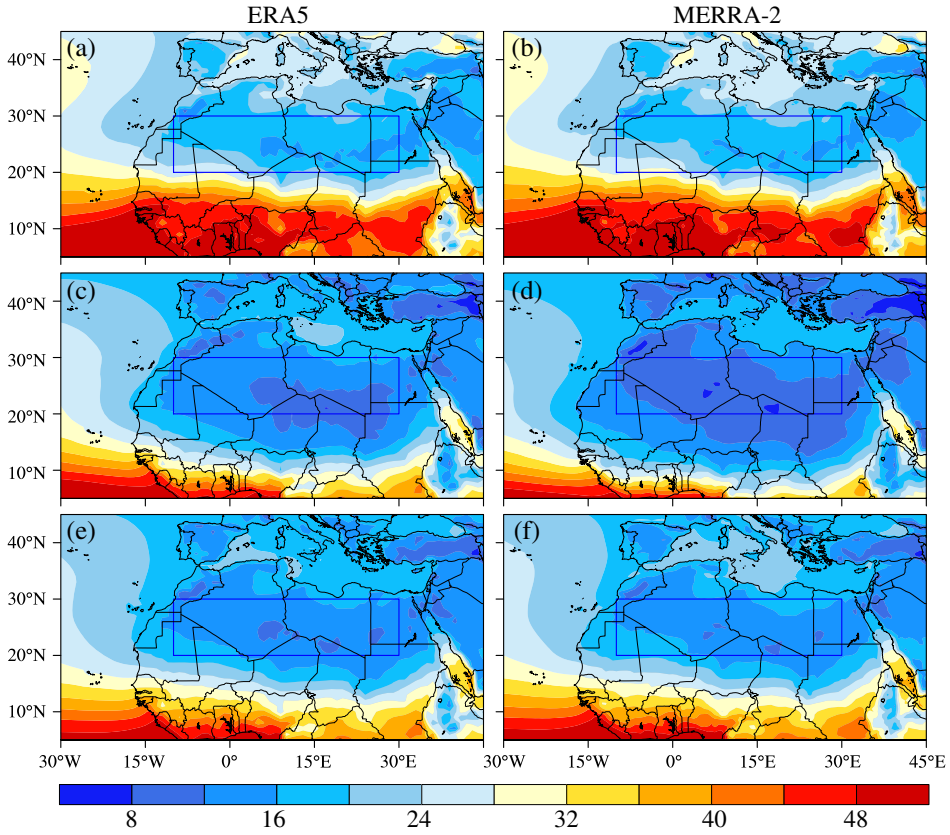


**FIGURE 1** Climatological JJA (a, b), DJF (c, d) and annual (e, f) TPW ($kg \cdot m^{-2}$) for ERA5 (left) and MERRA-2 (right). The rectangle boxes (20° – 30°N and 10°W–30°E) represents the boundaries of the Sahara Desert [Colour figure can be viewed at wileyonlinelibrary.com]

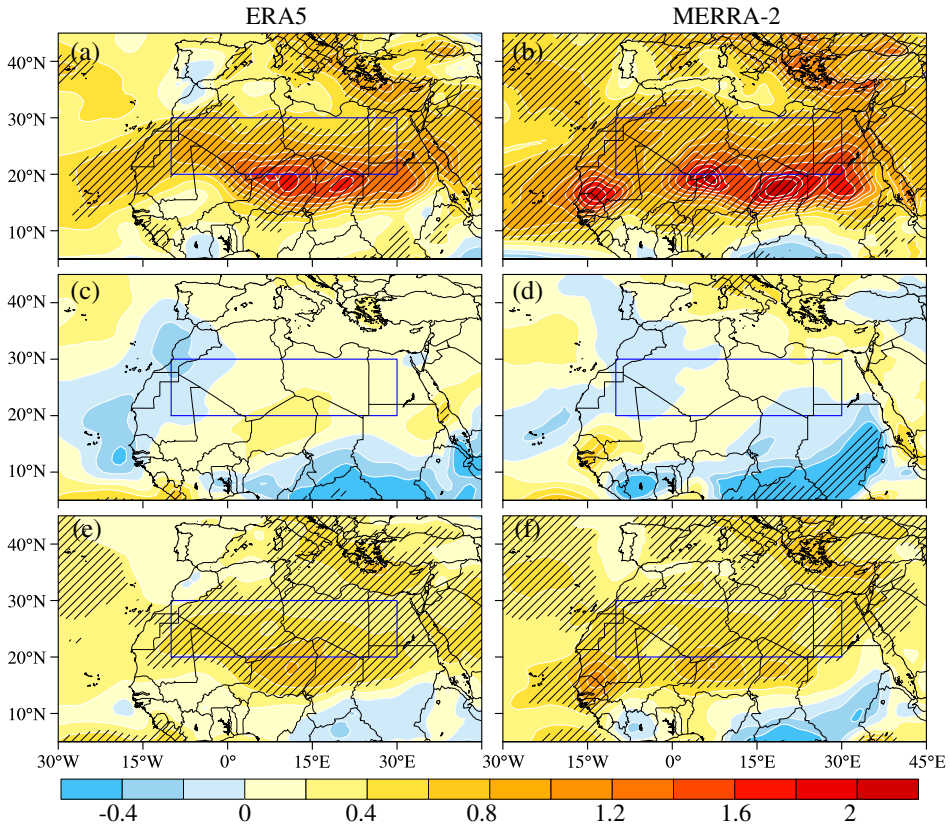


**FIGURE 2** JJA (a, b), DJF (c, d) and annual (e, f) trends of TPW ($kg \cdot m^{-2} \cdot decade^{-1}$) for ERA5 (left) and MERRA-2 (right). The area slashed denotes the region with significance of TPW trends at the 99% level of confidence. The rectangle boxes (20° – 30°N and 10°W–30°E) represents the boundaries of the Sahara Desert [Colour figure can be viewed at wileyonlinelibrary.com]

b,e,f). Such similarity indicates that the moistening over the Sahara Desert mainly takes place in JJA, which is in agreement with Vizy and Cook (2017). We have also examined the trends of TPW in boreal spring and autumn and find that TPW shows no significant changes in the boreal spring, while in the boreal autumn TPW displays relatively weaker positive trends over parts of the Sahara Desert (figures now shown). Overall, the consistency in two datasets illustrates that the Sahara Desert has been indeed experiencing a significant moistening in JJA since 1981 and bolsters our confidence in further analysis.

Since the increase of TPW mainly occurs in JJA, our subsequent analysis will focus only on the boreal summer. Figure 3 shows the water vapour content trends at different layers from two datasets. Similar to TPW, ERA5 and MERRA-2 are overall in good agreement with each other in terms of the moisture content trends at different layers over the Sahara Desert. In the lower troposphere below 900 hPa (Figure 3a,b), the trends of moisture content in ERA5 and MERRA-2 are positive and statistically significant over most areas of the Sahara Desert, even though the strongest moistening takes place south in the location of the monsoon trough (Thorncroft *et al*., 2011; Cook and Vizy, 2015; Vizy and Cook, 2017). The water vapour content between 900 and 700 hPa also displays statistically significant positive trends over the Sahara Desert, with the associated magnitude even larger than that in the lower troposphere below 900 hPa (Figure 3a–d). For the layer between 700 and 500 hPa, the trends of the water vapour content over the Sahara are still overall positive and statistically significant (Figure 3e,f). This suggests that the increase of moisture over the Sahara Desert in JJA is not confined to the lower troposphere but extends to the middle troposphere. In addition, the mechanism responsible for the moistening in the lower troposphere may differ from that in the middle troposphere.

To further quantitatively assess the vertical profile of the moistening rates over the Sahara Desert, here we calculate the area average $q$ trends at different pressure levels over the Sahara Desert in JJA from the two reanalysis datasets (Figure 4). One can see that the vertical profile of the area average $q$ trend over the Sahara Desert in ERA5 is similar to that in MERRA-2 to some extent. Moistening statistically significant at the 99% confidence level extends upwards to 400 hPa in ERA5 and 500 hPa in MERRA-2. This further testifies that the increase of water vapour content over the Sahara Desert in JJA occurs from the lower to middle troposphere.

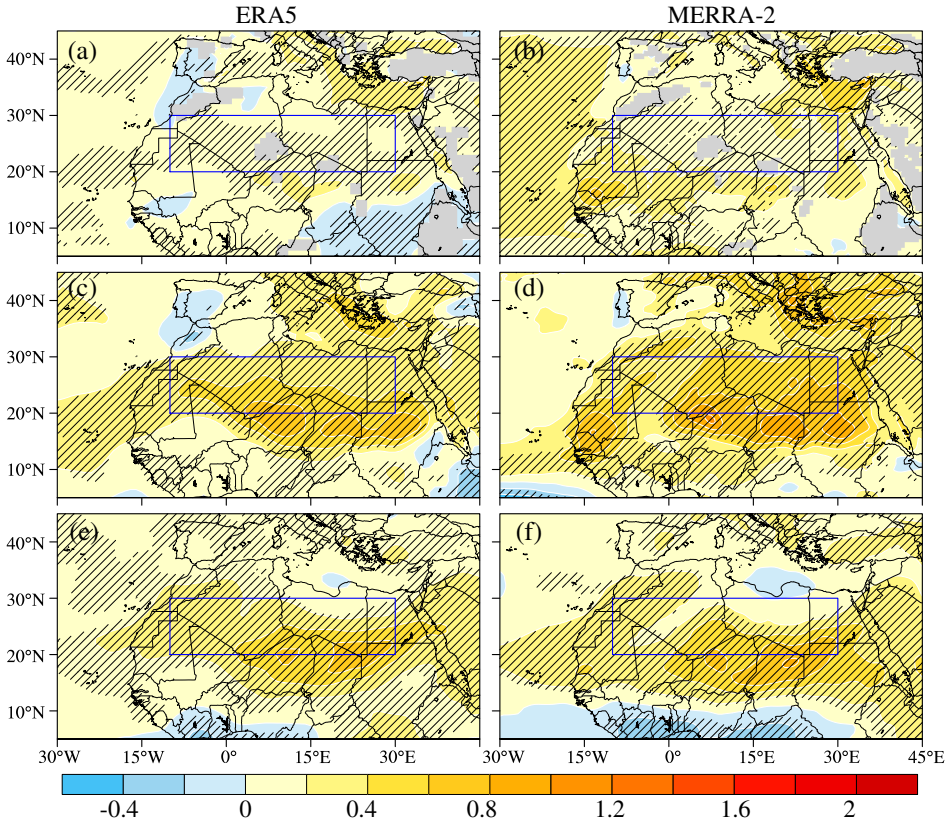


**FIGURE 3** JJA trends of TPW ($kg \cdot m^{-2} \cdot decade^{-1}$) from the surface to 900 hPa (a, b), 900–700 hPa (c, d) and 700–500 hPa (e, f) for ERA5 (left) and MERRA-2 (right). The area slashed denotes the region with significant TPW trends at the 90% level of confidence. The rectangle boxes (20° – 30°N and 10°W–30°E) represents the boundaries of the Sahara Desert [Colour figure can be viewed at wileyonlinelibrary.com]

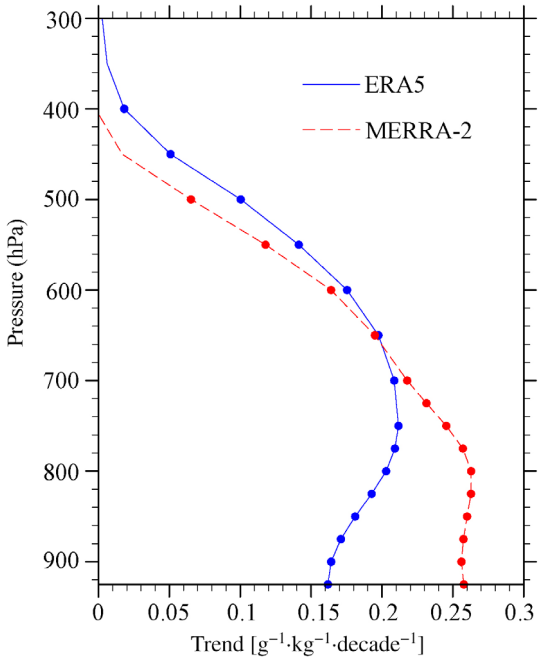


**FIGURE 4** The vertical profile of the area average JJA $q$ trend ($g^{-1}\cdot kg^{-1}\cdot decade^{-1}$) over the Sahara Desert. The dots denote significance of $q$ trends at the 99% level of confidence [Colour figure can be viewed at wileyonlinelibrary.com]

## 3.2 | Water vapour budget analysis for the Sahara Desert

To quantify the contributions of different physical processes to the moistening of the atmosphere over the Sahara Desert in JJA, in this section we will conduct the water vapour budget analysis for the atmosphere over the desert. By combining with Equations (2) and (4), Equation (1) can be written as

$$\frac{1}{g}\frac{\partial}{\partial t}\int_{p_t}^{p_s} q dp = F_{\text{north}} + F_{\text{south}} + F_{\text{east}} + F_{\text{west}} + E - P + R. \quad (6)$$

The results of the water vapour budget and the trends of each term are listed in Table 1. ERA5 and MERRA-2 generally agree well with each other in both the values and trends of each term. Table 1 highlights that the moisture transport across the northern boundary dominates the contribution to the increase of the moisture content, as the values and trends of $F_{\text{north}}$ are largest in both ERA5 and MERRA-2. While the northern boundary is the import channel, other boundaries are all the export channels, with only the eastern boundaries display a statistically significant trend. It is noteworthy that the moisture transport across each boundary is all of an order magnitude larger than the evaporation, precipitation and residual terms, which is expected as the evaporation and precipitation are

**TABLE 1** Climatological water vapour budget values ($mm\cdot day^{-1}$) and trends ($mm\cdot day^{-1}\cdot decade^{-1}$; in parentheses) for ERA5 (column 2) and MERRA-2 (column 3)

| | ERA5 | MERRA-2 |
|---|---|---|
| $F_{\text{north}}$ | 2.31 (***0.141***) | 2.49 (***0.145***) |
| $F_{\text{south}}$ | −1.54 (−0.016) | −1.56 (−0.0155) |
| $F_{\text{east}}$ | −0.6 (***−0.055***) | −0.56 (***−0.129***) |
| $F_{\text{west}}$ | −0.35 (−0.091) | −0.55 (−0.008) |
| $E$ | 0.093 (***0.004***) | 0.08 (0.002) |
| $P$ | 0.032 (***0.006***) | 0.036 (***0.01***) |
| $R$ | 0.09 (0.008) | 0.14 (0.005) |

*Note*: Statistically significant values at the 99% confidence level are italicized and boldfaced.

rather small over the hot dry desert (Figure S1, Supporting Information). Even though the evaporation and precipitation show statistically significant trends, the trends are much smaller than those of the moisture transport across the four boundaries. It is noteworthy that evaporation displays trends with different significance levels in the two reanalysis datasets, possibly due to the different soil moisture in ERA5 and MERRA-2. Exploring the relationship between the difference in soil moisture and evaporation is beyond the scope of this paper and will be a potential subject of future studies. Since it is the moisture transport across the four boundaries that dominate the moisture variability over the Sahara Desert, we will focus on the water vapour transport next.

### 3.2.1 | Climatological moisture transport in JJA

Figure 5 shows the moisture transport and geopotential height climatology in JJA over the Sahara Desert for ERA5. We have examined the climatology in MERRA-2 as well and the results are similar (figures not shown). In the lower troposphere in JJA, the northern African land is characterized by a monsoon trough centred around the Sahel (Figure 5a). The trough is converged by the northward moisture advection associated with the African monsoon to the south and the southward moisture transport accompanying the weak ridge across the Mediterranean Sea. The induced water vapour convergence can well explain the strong moistening in the Sahel (Figures 2a,b and 3). This climatological circulation pattern is consistent with previous studies (Thorncroft *et al.*, 2011; Neupane and Cook, 2013; Vizy *et al.*, 2013; Cook and Vizy, 2015).

Figure 5a highlights two branches of inward moisture transport into the Sahara Desert in the lower troposphere in JJA. One is the northerly moisture transport brought by the weak ridge across the Mediterranean Sea, another branch is

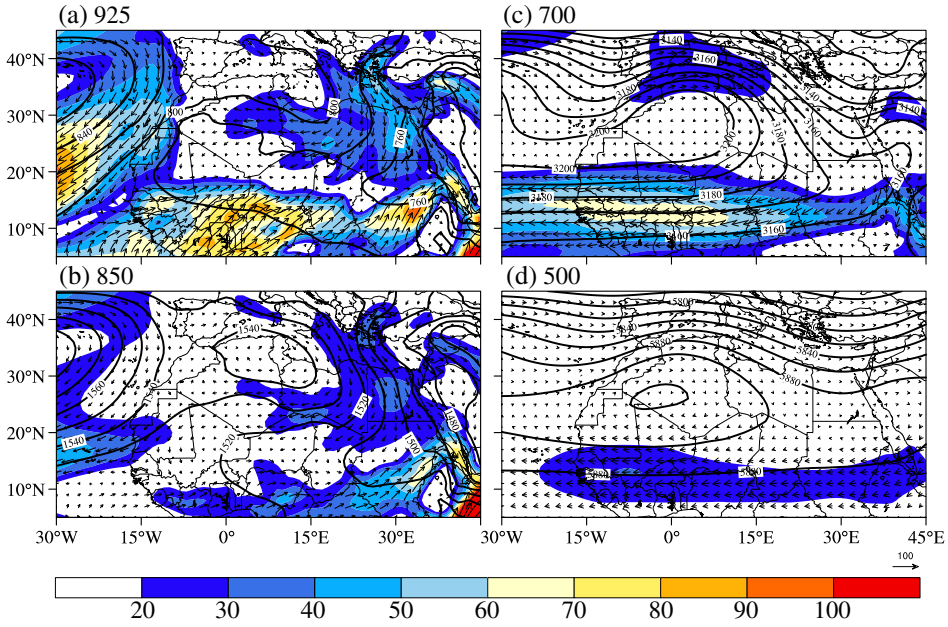


**FIGURE 5** Climatological moisture transport $q\vec{V}$(vectors; (g/kg) *(m/s)), its magnitude (shading), and geopotential height (contours; m) for 925 hPa (a), 850 hPa (b), 700 hPa (c) and 500 hPa (d) over JJA from 1981 to 2020 for ERA5 [Colour figure can be viewed at wileyonlinelibrary.com]

the southerly moisture transport related to the African monsoon. However, the northward African monsoon seems to be only able to reach around 18°N (Figure 5a), which agrees well with previous work (Lélé and Leslie, 2016). Even though the climatology may mask some extreme cases, this climatological circulation pattern implies to some extent that the contribution from the African monsoon to the increase of moisture content over the Sahara Desert in JJA may be small, though it indeed plays an important role in the Sahelian rainfall (Akinsanola and Zhou, 2019a; 2019b).

The circulation pattern mentioned above, with a monsoon trough to the south and a weak ridge to the north, extends upwards to around 850 hPa, as the weak cyclonic circulation can also be detected south of 20°N while the weak ridge to the north becomes a high with a closed circulation (Figure 5b). Above 850 hPa, the circulation climatology over the northern African land is characterized by an overwhelming Saharan high (Figure 5b–d). South of the Saharan high is the African easterly jet (Cook, 1999), which strongly intensifies the magnitude of the westward moisture transport over Sahel. The jet can also be detected at much higher levels on 500 hPa at the southern boundary of the subtropical high (Figure 5d).

Similar to the weak ridge at the lower troposphere (Figure 5a), the Saharan high at higher levels consistently transports the moisture from the Mediterranean Sea southward into the Sahara Desert via the northerly flow (Figure 5b–d). On the contrary, the northward moisture flux related to the African monsoon gradually diminishes with height (Figure 5a–d), which means that the moisture brought in by the monsoon is confined to the lower troposphere. The comparison between these two types of moisture transport suggests that the southward moisture transport associated with the Saharan high in the middle troposphere and weak ridge in the lower troposphere may play a much more important role in the moistening of the atmosphere over the Sahara Desert in JJA than the northward African monsoon does. This is consistent with the results of the water vapour budget, which indicates that the increased moisture mainly comes from the northern boundary while the southern boundary is an export channel (Table 1).

In summary, there are two branches of inward flow that transports water vapour into the Sahara Desert in JJA. One is associated with the northward African monsoon at the southern boundary in the lower troposphere, another is related to the ridge (Saharan high) at the northern boundary. The contribution of the former is expected to be much smaller than the latter.

### 3.2.2 | Moisture flux across each boundary

Figure 6 displays the climatology of the integrated water vapour transport (IVT) and the moisture fluxes at each boundary for ERA5 (a) and MERRA-2 (b) in JJA. Here IVT is defined following previous studies on atmospheric rivers (Mundhenk *et al.*, 2016; Kamae *et al.*, 2017; Zavadoff and Kirtman, 2020; Zhou *et al.*, 2021a),

$$\mathrm{IVT}=\frac{1}{g}\int_{p_t}^{p_s} q\vec{V}dp, \tag{7}$$

where $g$, $p_s$, $p_t$, $\vec{V}$, $q$ are defined in section 2. The spatial pattern of IVT in ERA5 (Figure 6a) is similar to that in

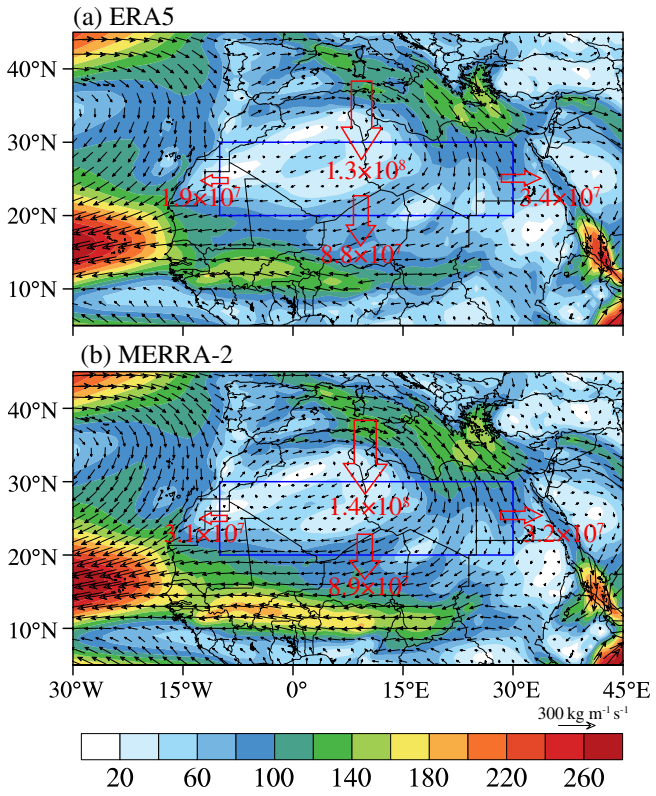


**FIGURE 6** Climatology of IVT (vectors; $kg \cdot m^{-1} \cdot s^{-1}$) and its magnitude (shading) in summer for ERA5 (a) and MERRA-2 (b) from 1981 to 2020. The arrows and values represent the direction and magnitude of moisture flux for each boundary ($kg \cdot s^{-1}$) [Colour figure can be viewed at wileyonlinelibrary.com]

MERRA-2 (Figure 6b), as both highlights a branch of northerly inward moisture flux associated with the Saharan high at the northern boundary of the Sahara Desert (Figures 5b–d and 6a,b). It is also noteworthy that the signal of the northward African monsoon at lower levels totally disappears in the spatial pattern of IVT south of the Sahara Desert (Figures 5a and 6a,b). This illustrates that the African easterly jet, the direction of which is almost opposite to that of the low-level African monsoon (Figure 5), dominates the moisture flux in JJA over the Sahel.

Following Equation (3), here we calculate the moisture flux for each boundary of the Sahara Desert for ERA5 (a) and MERRA-2 (b), the direction and intensity of the moisture fluxes are also shown in Figure 6 (arrows and numbers in red). Again, ERA5 and MERRA-2 exhibit similar moisture flux across the four boundaries in terms of magnitude and direction, except for the western boundary (Figure 6a,b). From Figure 6, one can see that for the Sahara Desert, the incoming moisture channel is at the northern boundary, while the west, south and east boundaries are all export channels, which is consistent with the results of the water vapour budget (Table 1). Obviously, the intensity of the inward moisture fluxes at the northern boundary is an order of magnitude larger than those outward moisture fluxes at other boundaries (Figure 6a,b). This indicates that the southward moisture flux associated with the Saharan high (weak ridge at lower levels) is the main contributor to the increased water vapour content over the Sahara Desert in JJA, and the Mediterranean Sea is one of the most important moisture supply sources for the increasing moisture over the Sahara Desert.

To test the robustness of our results, we have also moved the southern boundaries further southward and found that the results are similar (figures not shown). Another feature of interest is the difference of the moisture flux across the western boundary between ERA5 (Figure 6a) and MERRA-2 (Figure 6b). This difference is related to the different West African westerly jet (WAWJ) in the two reanalysis datasets. As shown in Figure 6b, MERRA-2 displays stronger WAWJ and thus larger moisture flux at the western boundary than ERA5, which can well explain the significant moistening trend around the west coastline of the African land in MERRA-2 (Figure 2b,f). Previous studies indicated that WAWJ plays a key role in the moisture transport and rainfall variability over West Africa during the boreal summer (Pu and Cook, 2012; Liu *et al.*, 2020). It is meaningful to explore the differences of WAWJ in the two reanalysis datasets, which, however, is beyond the scope of this paper and will be a subject of future studies.

Figure 7 displays the interannual variability of the moisture fluxes across each boundary. The two reanalysis datasets exhibit similar interannual variability and comparable trends of the moisture fluxes except for the western boundary (Figure 7a–d). Figure 7 highlights the statistically significant ($p < .01$) moisture inflow and outflow transport at the northern and eastern boundary respectively, while the trends of the moisture flux at the southern and western boundaries are statistically insignificant (Figure 7a,b). It is also noteworthy that the magnitudes of the inward moisture flux trends at the northern boundary in both reanalysis datasets are larger than the corresponding magnitudes of the outward moisture flux trend at the eastern boundary (Figure 7a,b). This demonstrates that the moisture content transported inward via the northerly inflow across the northern boundary is increasing at a much faster rate than the moisture content transported outward across the eastern boundary, which is responsible for the moistening of the atmosphere over the Sahara Desert in JJA and consistent with the results of the water vapour budget (Table 1).

To further elucidate the relationships between the moisture fluxes with the large-scale systems, here we study the vertical profiles of the climatological moisture transport (contours) and the associated trends (shadings) at each boundary (Figure 8). Similar to previous analyses,

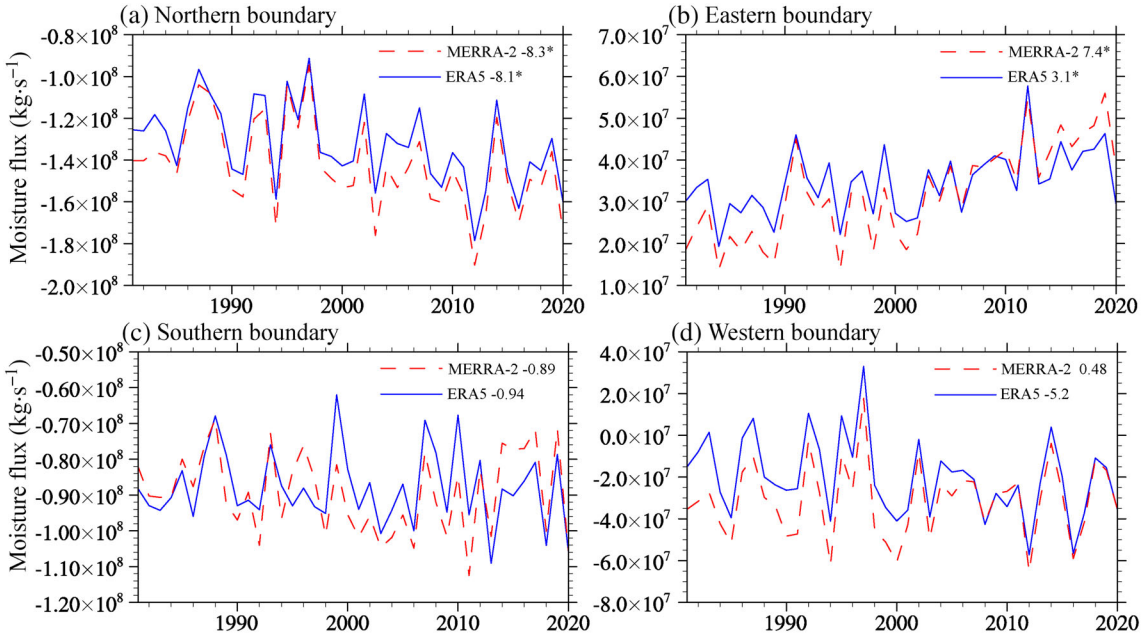


**FIGURE 7** Interannual variation of summer moisture fluxes across (a) northern, (b) eastern, (c) southern and (d) western boundary from ERA5 and MERRA-2. The associated numbers in the figure legend denote the trends ($10^6$ kg·s$^{-1}$·decade$^{-1}$). Trends statistically significant at the 99% level of confidence are labelled with "*" [Colour figure can be viewed at wileyonlinelibrary.com]

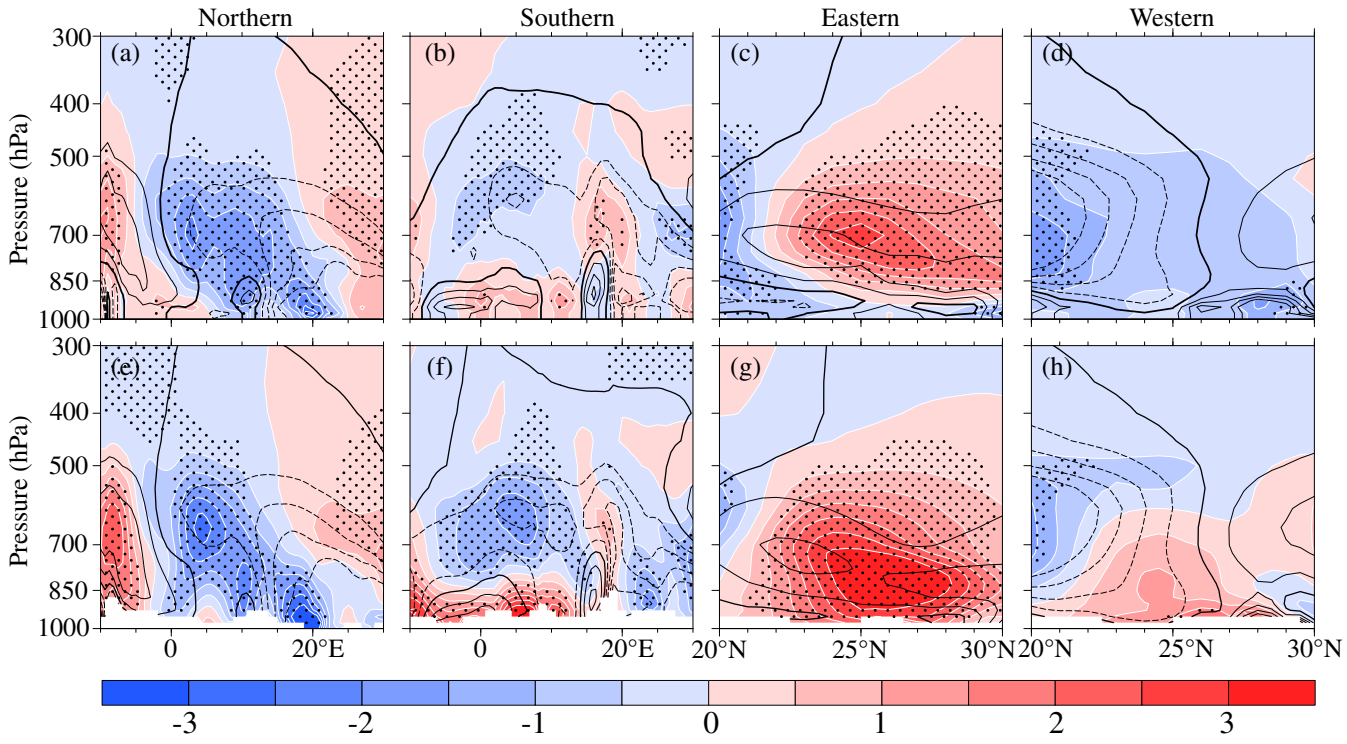


**FIGURE 8** Vertical cross section of the trends of moisture transport (shading; (g/kg)*(m/s)*decade$^{-1}$) and climatology moisture transport (contours; positive values denoted by solid lines and negative values denoted by dashed lines; (g/kg)*(m/s)) for the northern (a, e), southern (b, f), eastern (c, g) and western (d, h) boundary from ERA5 (a–d) and MERRA-2 (e–h). In the northern (a, e) and southern (b, f) boundaries, solid (positive) lines represent southerly moisture flux. In the eastern (c, g) and western (d, h) boundaries, solid (positive) lines represent westerly moisture flux. Stippling denotes significance of the moisture flux trends at the 95% level of confidence [Colour figure can be viewed at wileyonlinelibrary.com]

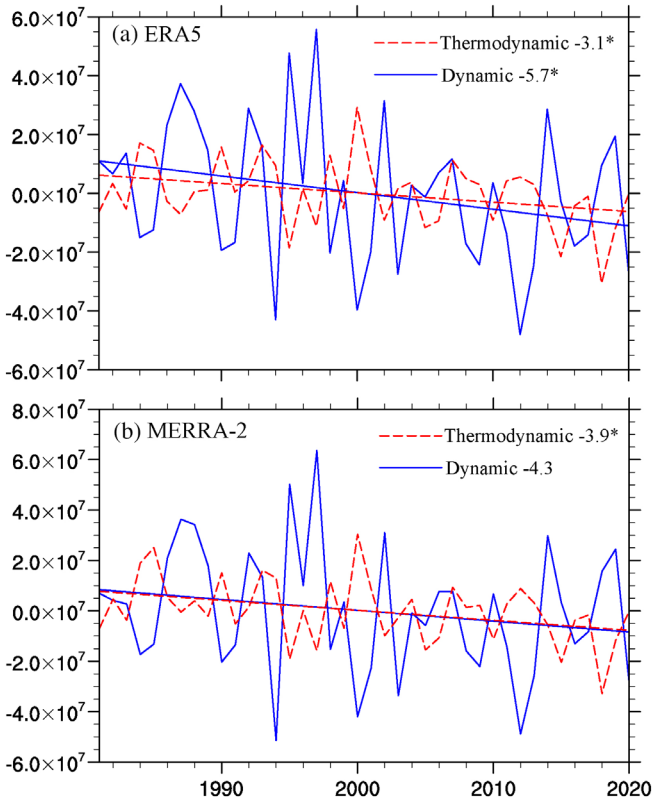


**FIGURE 9** Interannual variation of the moisture flux at the northern boundary caused by dynamic and thermodynamic term from (a) ERA5 and (b) MERRA-2. The associated numbers in the figure legend denote the trends ($10^6$ kg·s$^{-1}$·decade$^{-1}$). Trends statistically significant at the 90% level of confidence are labelled with "*" [Colour figure can be viewed at wileyonlinelibrary.com]

ERA5 and MERRA-2 exhibit similar vertical profile patterns of the climatological moisture transport and the associated trends except for the western boundary, where below 600 hPa the moisture transport trends in MERRA-2 and ERA5 are opposite (Figure 8d,h). However, both the trends in MERRA-2 and ERA5 below 600 hPa at the western boundary are statistically insignificant and thus will not matter that much in our study (Figure 8d,h).

Figure 8a,e highlights that the northern boundary is dominated by the northerly inward moisture fluxes from the prime meridian to 20°E, while the part west of prime meridian is characterized by the southerly outward moisture flux, which is related to the southerly flow of the Saharan high and the ridge (Figure 5). The dominant northerly moisture transport at the northern boundary is associated with the ridge and Saharan high to the north (Figure 5). Of particular importance is that the northerly inward moisture transport at the northern boundary is mostly characterized by a statistically significant negative (intensifying) trend (Figure 8a,e). The negative trend of the northerly moisture transport is characterized by two local maximums, with one in the lower troposphere at about 20°E and another in the middle troposphere (700 hPa) at the prime meridian (Figure 8a,e). This suggests that the northerly inward moisture transport associated with the ridge and the Saharan high above are both intensifying, contributing to the increase of the water vapour content over the Sahara Desert (Figure 5). Another fact of interest is that the maximum of the northerly moisture transport tilts westward with the height (Figure 8a,e), indicating a displacement between the ridge at lower levels and the Saharan high above. The displacement can also be slightly detected in Figure 5, as the closed Saharan high above the lower troposphere is located west of the ridge in the lower troposphere.

The vertical profiles of the moisture fluxes at other boundaries are also consistent with the circulation patterns shown in Figure 5. At the southern boundary (Figure 8b,f), one can see the shallow northward moisture transport related to the African monsoon in the lower troposphere, which may contribute some amounts of moisture in the atmosphere over the Sahara Desert. However, such moisture transport is confined to the lower troposphere. Above this shallow northward moisture transport related to the African monsoon, the southern boundary is overall characterized by the northerly moisture flux associated with the Saharan high, which also features an increasing trend in the middle troposphere (Figure 8b,f). As a result, the overall moisture flux across the whole southern boundary is still southward (Figure 6a,b), which further testifies that the contribution of the southerly moisture flux associated with the northward monsoon to the moistening of the atmosphere over the Sahara Desert is relatively small. The eastern boundary is characterized by the increasing outward westerly moisture flux related to the northwest flow circulating the Saharan high (Figure 5b–d), while the prominent feature in the western boundary is the increasing easterly moisture flux related to the easterly jet at about 20°N (Figure 5c,d). The intensifying easterly moisture flux signifies a strengthening African easterly jet, which is consistent with previous studies (Vizy and Cook, 2017).

In summary, the water vapour budget analysis demonstrates that most of the added moisture in JJA is transported into the Sahara Desert through the northern boundary via the northerly flow related to the Saharan high and the weak ridge, while the contribution from the African monsoon in the lower troposphere is relatively small. In addition, the northerly inward moisture transport is characterized by a statistically significant increasing trend, which drives the moistening of the atmosphere over the Sahara Desert in JJA.

### 3.3 | Dynamic and thermodynamic contributions to the increase and variability of the inward moisture transport across the northern boundary

As shown in the previous section, the moisture flux across the northern boundary is increasing since 1981, which is the key contributor to the moistening of the atmosphere in JJA over the Sahara Desert. The reason for such increase can be either attributable to the intensification of the wind or the increase of $q$ at the northern boundary. To further investigate which dominates the increase of the inward moisture flux at the northern boundary, here we decompose the moisture flux at the northern boundary into dynamic and thermodynamic terms following Equation (5). In addition, the interannual variability of the inward moisture flux is also examined.

The interannual variations in the decomposition of the moisture flux across the northern boundary for ERA5 (a) and MERRA-2 (b) are given in Figure 9. From Figure 9a,b, one can see that dynamic term (blue) exhibits larger variability than the thermodynamic term (red) does. Of particular importance is that the variability of the dynamic term is very close to that of the northern moisture flux (Figure 7a). For ERA5, the correlation coefficient between the dynamic term and the total moisture flux at the northern boundary is 0.91, which is statistically significant ($p < .0001$). On the contrary, the correlation coefficient between the thermodynamic term and the total moisture flux at the northern boundary is only about −0.2 and not statistically significant. The corresponding correlation coefficients in MERRA-2 is 0.87 ($p < .0001$) and −0.06 ($p > .1$), respectively (Figure 9b). This indicates that the interannual variability of the moisture flux at the northern boundary is mainly controlled by the dynamic term. In other words, the changes of the circulation patterns dominate the variability of the inward moisture flux at the northern boundary.

Another consensus between the two datasets highlighted in Figure 9 is that both the thermodynamic and dynamic terms have shown a tendency towards negative since 1981, and the trends of the dynamic terms are larger than those of thermodynamic terms, even though the trend of the dynamic term in MERAA2 is not statistically significant. This indicates that both the dynamic and thermodynamic processes contribute to the increase of the inward moisture transport at the northern boundary. Note that the values of the inward moisture flux at the northern boundary are negative as the inward flux flows from north to south (Figure 7a). The thermodynamic process involves the increase of specific humidity against fixed circulation patterns. Seager *et al.* (2010) attributes such increase primarily to the water vapour feedback in a warming climate under a fixed relative humidity. Here we examined the specific humidity and relative humidity at 925 hPa and found

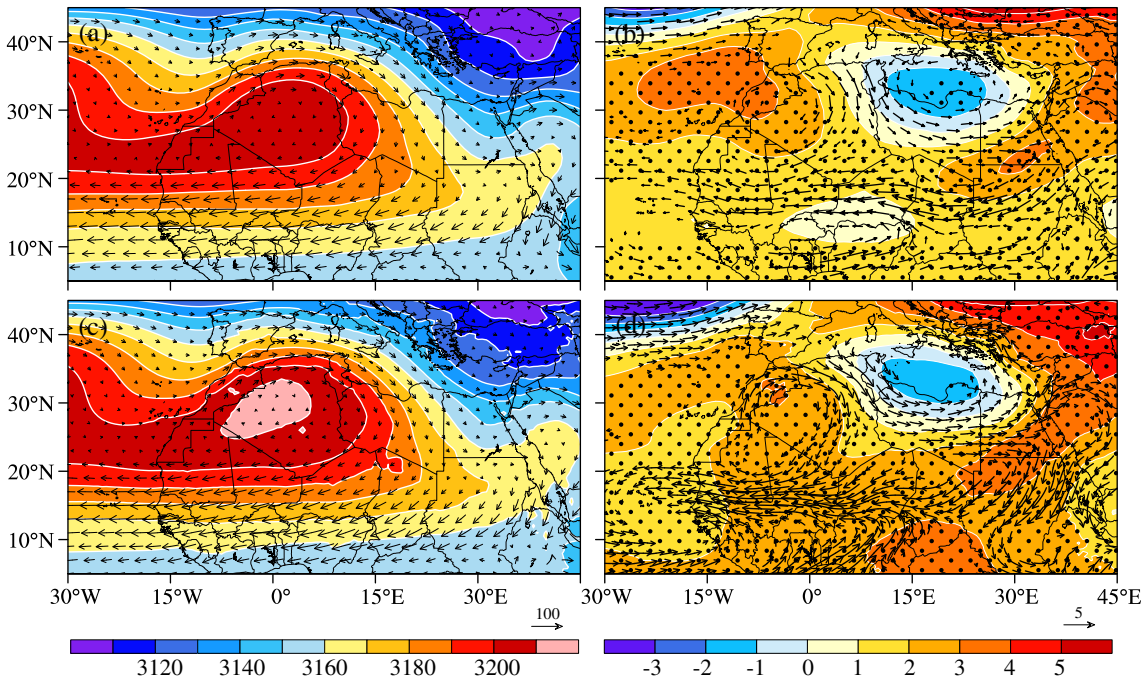


**FIGURE 10** 700 hPa summer climatological geopotential heights (shading; m) and moisture transport (vectors; (g/kg)*(m/s)) for (a) ERA5, (c) MERRA-2. Also shown are the 700 hPa summer geopotential heights trend (shading; m·decade$^{-1}$) and moisture transport trend (vectors; (g/kg)*(m/s)*decade$^{-1}$) significant at 90% level of confidence for (b) ERA5, (d) MERRA-2. Stippling denotes significance of geopotential heights trends at the 95% level of confidence [Colour figure can be viewed at wileyonlinelibrary.com]

that the relative humidity at the northern boundary indeed exhibits no significant changes (figure not shown), which is expected considering the large warming associated with the DA and the lack of local moisture availability. The little change in RH and the increase in specific humidity over the desert is primarily a result of moisture advection remotely from surrounding oceans. These results again indicate that the thermodynamic process may be dominated by the large-scale increasing specific humidity in a warming climate associated with the positive water vapour feedback, which is consistent with previous studies (Zhou *et al.*, 2016).

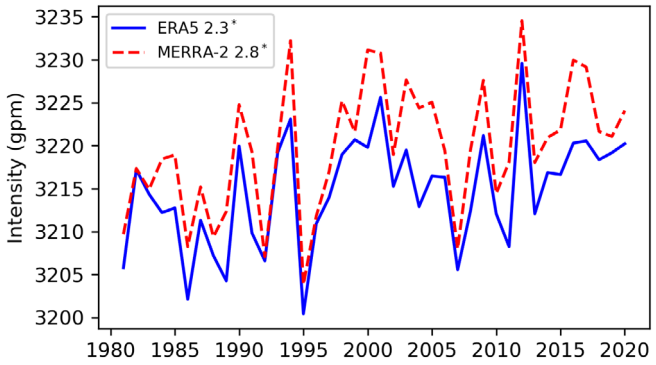


**FIGURE 11** Interannual variation of the Saharan high intensity for ERA5 and MERRA-2. The associated numbers in the figure legend denote the trends (gpm·decade$^{-1}$). Trends statistically significant at the 95% level of confidence are labelled with "*" [Colour figure can be viewed at wileyonlinelibrary.com]

Since the dynamic term also exhibits large contributions to the positive trend of the inward moisture flux at the northern boundary, here the changes of the circulation patterns from 1981 to 2020 over the Sahara Desert in JJA are examined. In the middle troposphere, the positive trends extending from the northeast African land to the Atlantic indicates a westward shift and expansion of the mid-level ridge and an intensifying Saharan high (Figure 10a–d). The intensification can also be detected via the trends of the moisture transport, with the enhanced northerly wind anomalies in both ERA5 and MERRA-2 in the northwest corner of the African land (Figure 10b,d). The increasing southward inward moisture transport accompanying the strengthening Saharan high at the northern boundary of the African land corresponds well to the midlevel maximum of the positive moisture flux trends in Figure 8a,e, which transports an increasing amount of water vapour into the atmosphere over the Sahara Desert.

To further testify the intensification of the Saharan high, we evaluate the intensity of the Saharan high quantitatively. Following Sun *et al.* (2017), here the intensity is defined as the maximum 700 hPa geopotential height over the area from 15° – 40°N and −15°W–30°E. The interannual variation of the intensity is given in Figure 11. Both ERA5 and MERRA-2 display statistically significant positive trends, indicating that the Saharan high has been strengthening from 1981 to 2020. We also examined the position and size of the Saharan high. The position is defined as the location of the geopotential height maximum. Following Sun *et al.* (2017), we scale

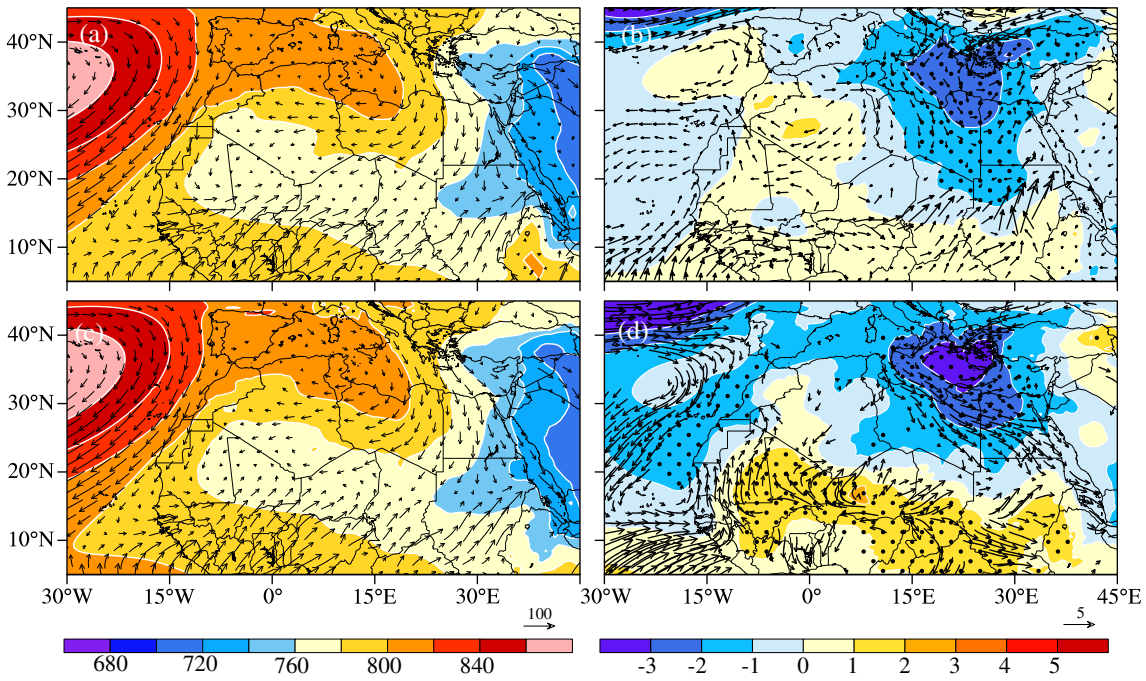


**FIGURE 12** As in Figure 10 but for 925 hPa [Colour figure can be viewed at wileyonlinelibrary.com]

the geopotential height and then choose 38 gpm anomalies to define the extent of the Saharan high (Figure S2). We found that the Saharan high has not moved (figure not shown) but indeed expanded significantly from 1981 to 2020 (Figure S3).

In the lower troposphere, MERRA-2 exhibits positive geopotential height trends south of 20°N and negative trends north of 20°N over the African land, pointing to a northward shift of the monsoon trough over the Sahel (Figure 12c,d), which is in agreement with previous studies (Shekhar and Boos, 2017; Vizy and Cook, 2017). Such a dipole pattern and the shift of the monsoon trough can also be detected in ERA5 (Figure 12a,b). Over the Mediterranean Sea, both ERA5 (Figure 12b) and MERRA-2 (Figure 12d) display statistically significant ($p < .05$) negative trends of geopotential heights. This is consistent with the results shown in Vizy and Cook (2017) and Skinner *et al*. (2012). These changes may reflect the westward extension of the low over the Arabian Peninsula (Figure 12a,b), which intensifies the magnitude of the accompanied northerly winds and thus brings more moisture from the Mediterranean Sea into the lower troposphere over the Sahara Desert. The area of the intensifying northerly moisture transport due to the westward extension of the low corresponds well spatially to the negative trends of moisture transport in the lower troposphere shown in Figure 8a,e, which constitutes the water vapour transport channel at lower levels. This suggests that the circulation change over the Arabian Peninsula may impact the Sahara Desert as well.

## 4 | CONCLUSIONS

Previous studies suggest that the Sahara Desert is experiencing a fast rate of warming (Cook and Vizy, 2015; Zhou *et al*., 2015; Zhou, 2016; Wei *et al*., 2017). Many studies have linked this warming to the enhanced downward longwave radiation associated with increasing amounts of water vapour over the desert (Evan *et al*., 2015; Zhou *et al*., 2016; Vizy and Cook, 2017). Aiming at answering two questions as to where the increased moisture over the Sahara Desert comes from and how do the thermodynamic and dynamic processes contribute relatively to the changes of the moisture transport, here we use two reanalysis datasets (ERA5 and MERRA-2) to do the moisture budget over the Sahara Desert from 1981 to 2020. We find that the atmosphere over the Sahara Desert has been experiencing a significant moistening since 1981, and such increase of moisture mainly takes place in JJA. The moistening is not confined to the lower troposphere, but extends upwards to the middle troposphere.

The climatology of the moisture transport shows that in the lower troposphere over the Sahara Desert in JJA, there are two branches of inward water vapour flux, one is associated with the northward African monsoon and the other is related to the weak ridge across the Mediterranean Sea to the north. In the middle troposphere, the main water vapour channel is the northerly moisture transport related to the Saharan high, while the northward African monsoon is confined to the lower troposphere and is absent in the middle troposphere. The water vapour budget analysis indicates that the northern boundary is the main channel through which the moisture is transported into the Sahara Desert via the northerly inward moisture flux accompanying the weak ridge in the lower troposphere and Saharan high in the middle troposphere, while the other boundaries are the export channels. Additionally, the northerly moisture flux across the northern boundary is increasing at a faster rate than the outward moisture flux at other boundaries, driving the net increase of moisture over the Sahara Desert in JJA.

The decomposition of the northerly moisture flux shows that the interannual variability of the increasing inward moisture flux at the northern boundary is dominated by the dynamic process. However, both dynamic and thermodynamic processes contribute to the increasing trend of the inward water vapour transport at the northern boundary. The thermodynamic process is attributed to the overall large-scale increase of specific humidity in a warming climate associated with the positive water vapour feedback, while the dynamic process is linked to the circulation pattern changes that intensify the northerly moisture flux at the northern boundary. Further trend analysis shows that in the middle troposphere, the increasing northerly moisture transport is associated with the intensifying Saharan high. In the lower troposphere, the increased northerly water vapour transport is linked to the westward extension of the low over the Arabian Peninsula. These two changes all strengthen the northerly winds and thus favour the increase of the inward moisture transport at the northern boundary. This indicates that the Mediterranean Sea may be an important source of moisture for the Sahara Desert.

However, it is still possible that the moisture comes from the Atlantic Ocean, or the Indian Ocean. Further analysis of the origin of the increased moisture over the Sahara Desert needs to trace the path of the water vapour, which involves the use of models and will be a subject of future work. In addition, previous studies have shown that in the boreal summer, there exist some remote influences on the Sahara Desert, such as the Indian monsoon (Rodwell and Hoskins, 1996). Such remote control on the moisture and its transport is not clear and still needs further research. It is also possible that the moisture content change in the middle troposphere over the Sahara Desert may be related to the

change of cloud cover over the desert. Given the uncertainty of the cloud cover in the data and models, this relationship still needs further in-depth research. Additionally, significant regional variability in moisture transport may also exist in the Sahara Desert, which will also be the potential subject of future studies.

## ACKNOWLEDGEMENTS

This research is supported by the National Science Foundation (NSF) (AGS-1952745). We thank Dr. Samar Minallah for sharing the code on the water vapour budget. Gratitude is also extended to Dr. Edward K. Vizy for the help on calculating the moisture transport trends. We sincerely thank Dr. Brian Rose for the insightful discussions and comments that helped improve the quality of our work.

## AUTHOR CONTRIBUTIONS

**Li Zhuo:** Formal analysis; investigation; methodology; visualization; writing – original draft. **Liming Zhou:** Funding acquisition; supervision; writing – review and editing.

## ORCID

*Li Zhuo* https://orcid.org/0000-0002-7547-9162

## REFERENCES

Akinsanola, A.A. and Zhou, W. (2019a) Dynamic and thermodynamic factors controlling increasing summer monsoon rainfall over the West African Sahel. *Climate Dynamics*, 52, 4501–4514. https://doi.org/10.1007/s00382-018-4394-x.

Akinsanola, A.A. and Zhou, W. (2019b) Projections of West African summer monsoon rainfall extremes from two CORDEX models. *Climate Dynamics*, 52, 2017–2028. https://doi.org/10.1007/s00382-018-4238-8.

Cook, K.H. (1999) Generation of the African easterly jet and its role in determining West African precipitation. *Journal of Climate*, 12, 1165–1184. https://doi.org/10.1175/1520-0442(1999)012<1165:GOTAEJ>2.0.CO;2.

Cook, K.H. and Vizy, E.K. (2015) Detection and analysis of an amplified warming of the Sahara Desert. *Journal of Climate*, 28, 6560–6580. https://doi.org/10.1175/JCLI-D-14-00230.1.

Cook, K.H., Vizy, E.K., Liu, Y. and Liu, W. (2021) Greenhouse-gas induced warming amplification over the Arabian Peninsula with implications for Ethiopian rainfall. *Climate Dynamics*, 57, 3113–3133. https://doi.org/10.1007/s00382-021-05858-x.

Dai, L., Wright, J.S. and Fu, R. (2020) Moisture and energy budget perspectives on summer drought in north China. *Journal of Climate*, 33, 10149–10167. https://doi.org/10.1175/JCLI-D-20-0176.1.

Druyan, L.M. (2011) Studies of 21st-century precipitation trends over West Africa. *International Journal of Climatology*, 31, 1415–1424. https://doi.org/10.1002/joc.2180.

Evan, A.T., Flamant, C., Lavaysse, C., Kocha, C. and Saci, A. (2015) Water vapor-forced greenhouse warming over the Sahara Desert and the recent recovery from the Sahelian drought. *Journal of Climate*, 28, 108–123. https://doi.org/10.1175/JCLI-D-14-00039.1.

Gelaro, R., McCarty, W., Suárez, M. J., Todling, R., Molod, A., Takacs, L., Randles, C. A., Darmenov, A., Bosilovich, M. G., Reichle, R., Wargan, K., Coy, L., Cullather, R., Draper, C., Akella, S., Buchard, V., Conaty, A., da Silva, A. M., Gu, W., Kim, G., Koster, R., Lucchesi, R., Merkova, D., Nielsen, J. E., Partyka, G., Pawson, S., Putman, W., Rienecker, M., Schubert, S. D., Sienkiewicz, M., and Zhao, B. (2017) The modern-era retrospective analysis for research and applications, version 2 (MERRA-2). *Journal of Climate*, 30, 5419–5454. https://doi.org/10.1175/JCLI-D-16-0758.1.

Harada, C., Sumi, A. and Ohmori, H. (2003) Seasonal and year-to-year variations of rainfall in the Sahara desert region based on TRMM PR data. *Geophysical Research Letters*, 30, 6–9. https://doi.org/10.1029/2002GL016695.

Hersbach, H., Bell, B., Berrisford, P., Hirahara, S., Horányi, A., Muñoz-Sabater, J., Nicolas, J., Peubey, C., Radu, R., Schepers, D., Simmons, A., Soci, C., Abdalla, S., Abellan, X., Balsamo, G., Bechtold, P., Biavati, G., Bidlot, J., Bonavita, M., Chiara, G. D., Dahlgren, P., Dee, D., Diamantakis, M., Dragani, R., Flemming, J., Forbes, R., Fuentes, M., Geer, A., Haimberger, L., Healy, S., Hogan, R. J., Hólm, E., Janisková, M., Keeley, S., Laloyaux, P., Lopez, P., Lupu, C., Radnoti, G., Rosnay. P., Rozum, I., Vamborg, F., Villaume, S., Thépaut, J. N. (2020) The ERA5 global reanalysis. *Quarterly Journal of the Royal Meteorological Society*, 146, 1999–2049. https://doi.org/10.1002/qj.3803.

Jin, F., Kitoh, A. and Alpert, P. (2011) Climatological relationships among the moisture budget components and rainfall amounts over the Mediterranean based on a super-high-resolution climate model. *Journal of Geophysical Research: Atmospheres*, 116, 1–13. https://doi.org/10.1029/2010JD014021.

Kamae, Y., Mei, W., Xie, S.P., Naoi, M. and Ueda, H. (2017) Atmospheric rivers over the Northwestern Pacific: Climatology and interannual variability. *Journal of Climate*, 30, 5605–5619. https://doi.org/10.1175/JCLI-D-16-0875.1.

Lamb, P.J., Portis, D.H. and Zangvil, A. (2012) Investigation of large-scale atmospheric moisture budget and land surface interactions over U.S. southern great plains including for CLASIC (June 2007). *Journal of Hydrometeorology*, 13, 1719–1738. https://doi.org/10.1175/JHM-D-12-01.1.

Lélé, M.I. and Leslie, L.M. (2016) Intraseasonal variability of low-level moisture transport over West Africa. *Climate Dynamics*, 47, 3575–3591. https://doi.org/10.1007/s00382-016-3334-x.

Liu, W., Cook, K.H. and Vizy, E.K. (2020) Role of the West African westerly jet in the seasonal and diurnal cycles of precipitation over West Africa. *Climate Dynamics*, 54, 843–861. https://doi.org/10.1007/s00382-019-05035-1.

Mayer, J., Mayer, M. and Haimberger, L. (2021) Consistency and homogeneity of atmospheric energy, moisture, and mass budgets in ERA5. *Journal of Climate*, 34, 3955–3974. https://doi.org/10.1175/JCLI-D-20-0676.1.

Minallah, S. and Steiner, A.L. (2021) Role of the atmospheric moisture budget in defining the precipitation seasonality of the great lakes region. *Journal of Climate*, 34, 643–657. https://doi.org/10.1175/JCLI-D-19-0952.1.

Monerie, P.A., Biasutti, M. and Roucou, P. (2016) On the projected increase of Sahel rainfall during the late rainy season. *International Journal of Climatology*, 36, 4373–4383. https://doi.org/10.1002/joc.4638.

Mundhenk, B.D., Barnes, E.A., Maloney, E.D. and Nardi, K.M. (2016) Modulation of atmospheric rivers near Alaska and the U.S. west coast by Northeast Pacific height anomalies. *Journal*

*of Geophysical Research: Atmospheres*, 121, 12751–12765. https://doi.org/10.1002/2016JD025350.

Neupane, N. and Cook, K.H. (2013) A nonlinear response of Sahel rainfall to Atlantic warming. *Journal of Climate*, 26, 7080–7096. https://doi.org/10.1175/JCLI-D-12-00475.1.

Odoulami, R.C. and Akinsanola, A.A. (2018) Recent assessment of West African summer monsoon daily rainfall trends. *Weather*, 73, 283–287. https://doi.org/10.1002/wea.2965.

Pausata, F.S.R., Gaetani, M., Messori, G., Berg, A., Maia de Souza, D., Sage, R.F. and deMenocal, P.B. (2020) The greening of the Sahara: past changes and future implications. *One Earth*, 2, 235–250. https://doi.org/10.1016/j.oneear.2020.03.002.

Pu, B. and Cook, K.H. (2012) Role of the west African westerly jet in Sahel rainfall variations. *Journal of Climate*, 25, 2880–2896. https://doi.org/10.1175/JCLI-D-11-00394.1.

Rodwell, M.J. and Hoskins, B.J. (1996) Monsoons and the dynamics of deserts. *Quarterly Journal of the Royal Meteorological Society*, 122, 1385–1404. https://doi.org/10.1002/qj.49712253408.

Seager, R., Naik, N. and Vecchi, G.A. (2010) Thermodynamic and dynamic mechanisms for large-scale changes in the hydrological cycle in response to global warming. *Journal of Climate*, 23, 4651–4668. https://doi.org/10.1175/2010JCLI3655.1.

Shekhar, R. and Boos, W.R. (2017) Weakening and shifting of the Saharan shallow meridional circulation during wet years of the West African monsoon. *Journal of Climate*, 30, 7399–7422. https://doi.org/10.1175/JCLI-D-16-0696.1.

Skinner, C.B., Ashfaq, M. and Diffenbaugh, N.S. (2012) Influence of twenty-first-century atmospheric and sea surface temperature forcing on West African climate. *Journal of Climate*, 25, 527–542. https://doi.org/10.1175/2011JCLI4183.1.

Sun, B. and Wang, H. (2014) Moisture sources of semiarid grassland in China using the lagrangian particle model FLEXPART. *Journal of Climate*, 27, 2457–2474. https://doi.org/10.1175/JCLI-D-13-00517.1.

Sun, X., Cook, K.H. and Vizy, E.K. (2017) The South Atlantic subtropical high: climatology and interannual variability. *Journal of Climate*, 30, 3279–3296. https://doi.org/10.1175/JCLI-D-16-0705.1.

Thomas, N. and Nigam, S. (2018) Twentieth-century climate change over Africa: seasonal hydroclimate trends and Sahara Desert expansion. *Journal of Climate*, 31, 3349–3370. https://doi.org/10.1175/JCLI-D-17-0187.1.

Thorncroft, C.D., Nguyen, H., Zhang, C. and Peyrille, P. (2011) Annual cycle of the West African monsoon: regional circulations and associated water vapour transport. *Quarterly Journal of the Royal Meteorological Society*, 137, 129–147. https://doi.org/10.1002/qj.728.

Vizy, E.K. and Cook, K.H. (2017) Seasonality of the observed amplified Sahara warming trend and implications for Sahel rainfall. *Journal of Climate*, 30, 3073–3094. https://doi.org/10.1175/JCLI-D-16-0687.1.

Vizy, E.K., Cook, K.H., Crétat, J. and Neupane, N. (2013) Projections of a wetter Sahel in the twenty-first century from global and regional models. *Journal of Climate*, 26, 4664–4687. https://doi.org/10.1175/JCLI-D-12-00533.1.

Wang, S., Sobel, A.H., Zhang, F., Qiang Sun, Y., Yue, Y. and Zhou, L. (2015) Regional simulation of the October and November MJO events observed during the CINDY/DYNAMO field campaign at gray zone resolution. *Journal of Climate*, 28, 2097–2119. https://doi.org/10.1175/JCLI-D-14-00294.1.

Wang, Z., Duan, A., Yang, S. and Ullah, K. (2017) Atmospheric moisture budget and its regulation on the variability of summer precipitation over the Tibetan Plateau. *Journal of Geophysical Research: Atmospheres*, 122, 614–630. https://doi.org/10.1002/2016JD025515.

Wei, N., Zhou, L., Dai, Y., Xia, G. and Hua, W. (2017) Observational evidence for desert amplification using multiple satellite datasets. *Scientific Reports*, 7, 1–15. https://doi.org/10.1038/s41598-017-02064-w.

Zangvil, A., Portis, D.H. and Lamb, P.J. (2004) Investigation of the large-scale atmospheric moisture field over the midwestern United States in relation to summer precipitation. Part II: recycling of local evapotranspiration and association with soil moisture and crop yields. *Journal of Climate*, 17, 3283–3301. https://doi.org/10.1175/1520-0442(2004)017<3283:IOTLAM>2.0.CO;2.

Zavadoff, B.L. and Kirtman, B.P. (2020) Dynamic and thermodynamic modulators of European atmospheric rivers. *Journal of Climate*, 33, 4167–4185. https://doi.org/10.1175/JCLI-D-19-0601.1.

Zhou, L. (2016) Desert amplification in a warming climate. *Scientific Reports*, 6, 1–13. https://doi.org/10.1038/srep31065.

Zhou, L. (2021) Diurnal asymmetry of desert amplification and its possible connections to planetary boundary layer height: a case study for the Arabian Peninsula. *Climate Dynamics*, 56, 3131–3156. https://doi.org/10.1007/s00382-021-05634-x.

Zhou, L., Chen, H. and Dai, Y. (2015) Stronger warming amplification over drier ecoregions observed since 1979. *Environmental Research Letters*, 10, 64012. https://doi.org/10.1088/1748-9326/10/6/064012.

Zhou, L., Chen, H., Hua, W., Dai, Y. and Wei, N. (2016) Mechanisms for stronger warming over drier ecoregions observed since 1979. *Climate Dynamics*, 47, 2955–2974. https://doi.org/10.1007/s00382-016-3007-9.

Zhou, Y., Kim, H. and Waliser, D.E. (2021a) Atmospheric river lifecycle responses to the Madden–Julian Oscillation. *Geophysical Research Letters*, 48, 1–10. https://doi.org/10.1029/2020GL090983.

Zhou, L., Tian, Y., Wei, N., Ho, S.P. and Li, J. (2021b) Rising planetary boundary layer height over the Sahara Desert and arabian peninsula in a warming climate. *Journal of Climate*, 34, 4043–4068. https://doi.org/10.1175/JCLI-D-20-0645.1.

## SUPPORTING INFORMATION

Additional supporting information may be found in the online version of the article at the publisher's website.

**How to cite this article:** Zhuo, L., & Zhou, L. (2022). Moisture transport and water vapour budget over the Sahara Desert. *International Journal of Climatology*, 1–15. https://doi.org/10.1002/joc.7614